NANO LETTERS

pubs.acs.org/NanoLett Letter

Transparent and Robust Amphiphobic Surfaces Exploiting Nanohierarchical Surface-grown Metal−Organic Frameworks

Vikramjeet Singh, Xuehu Men, and Manish K. Tiwari*

Cite This: https://doi.org/10.1021/acs.nanolett.1c00157 Read Online

ACCESS | Metrics & More | Article Recommendations | Supporting Information

ABSTRACT: Highly amphiphobic (repelling both water and low surface tension liquids) and optically transparent surface treatments have widespread demand. By combining a rational growth of metal−organic frameworks (MOFs) with functionalization by environmentally safe, flexible alkyl groups, here we present surfaces with nanohierarchical morphology, comprising two widely differing nanoscale features. These nanohierarchical MOF films show excellent amphiphobicity. We further present three key features. First, we demonstrate the need to use flexible alkyl chains to achieve low drop sliding angles and self-cleaning. Second, our thin (~200 nm) MOF films display excellent optical transparency and robustness. Third, the nanohierarchical morphology enables a unique combination of additional desirable properties, e.g., resistance to high-speed liquid impact (up to ~35 m/s, Weber number >4 × 10^4), thermal stability up to 200 °C, scratch resistance, low ice adhesion for >10 icing/deicing cycles, stability in harsh acidic and basic environments, and capability to remove carcinogenic pollutants from water.

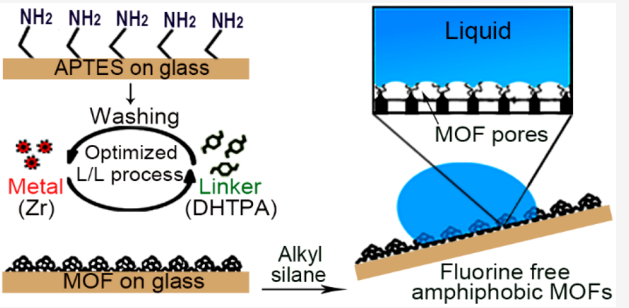

KEYWORDS: *Amphiphobic surface, metal−organic frameworks, ice adhesion, transparent surface, nanohierarchy, pollution cleaning*

Transparent amphiphobic surfaces, with an ability to repel low surface tension liquids, are of great interest in applications such as self-cleaning, antifouling, window panes, wind screens, water harvesting, condensation, anti-icing, etc.[1,2] On superamphiphobic surfaces, exploiting micro/nanoscale roughness engineering, simultaneously achieving all-round robustness and transparency, is nontrivial because enhancing roughness improves liquid repellency but worsens the transparency.[3] Despite notable reports on transparent superamphiphobic surfaces,[4−6] impalement resistance has only been demonstrated against droplet impacts and not against high-speed jets.[7] Closeness of surface asperities helps with (surface energy enabled) impalement resistance (due to smaller capillary radius);[3] however, it is challenging to produce mechanically robust nanotextures with a few-nanometer manufacturing precision, even with compromises in fabrication scalability. Alternatives such as liquid-infused or ultrasmooth surfaces show low hysteresis and slippery behavior but are unable to sustain high-speed liquid impact. Recently, Wang et al. developed an armor strategy to achieve mechanically robust, transparent superhydrophobic surfaces; however, amphiphobicity was not considered.[8] In a departure, here we exploit surface-grown metal−organic frameworks (MOFs)[9−11] to introduce a new mechanism of amphiphobicity without compromising on transparency, robustness, or liquid-impalement resistance. We achieve the amphiphobic feature by using MOFs films with a hierarchy of nanotextures (termed nanohierarchy) and rational, fluorine-free functionalization for environmental benefits. To demonstrate the proof-of-concept, we used common zirconium-based MOFs (Zr-MOFs or UIO-66-OH) and grew them directly onto prefunctionalized glass substrate (Figure 1A). The hydroxyl groups of the MOF linker were exploited for postfunctionalization with alkyl silanes. Zr-MOFs were used to benefit from their high chemical, thermal, and mechanical stable structure (minimum sheer modulus of 13.7 GPa)[12] arising from the high degree of coordination where each metal ion (Zr) is linked to 12 linkers.[13]

Hydrolytic susceptibility and moisture sensitivity of MOF particles and powders is a well-known challenge and widely researched. Typically, three strategies are used to overcome the challenge: using fluorinated linkers in MOF synthesis, postsynthetic modification with suitable hydrophobic monolayer, and coating hydrophobic polymers coatings.[14] Such hydrophobic MOFs have been exploited for a diversity of applications in energy storage, catalysis enhancement, and oil/water separation.[15] However, their full potential remains underutilized due to the brittle nature and poor processability

Received: January 13, 2021
Revised: March 15, 2021

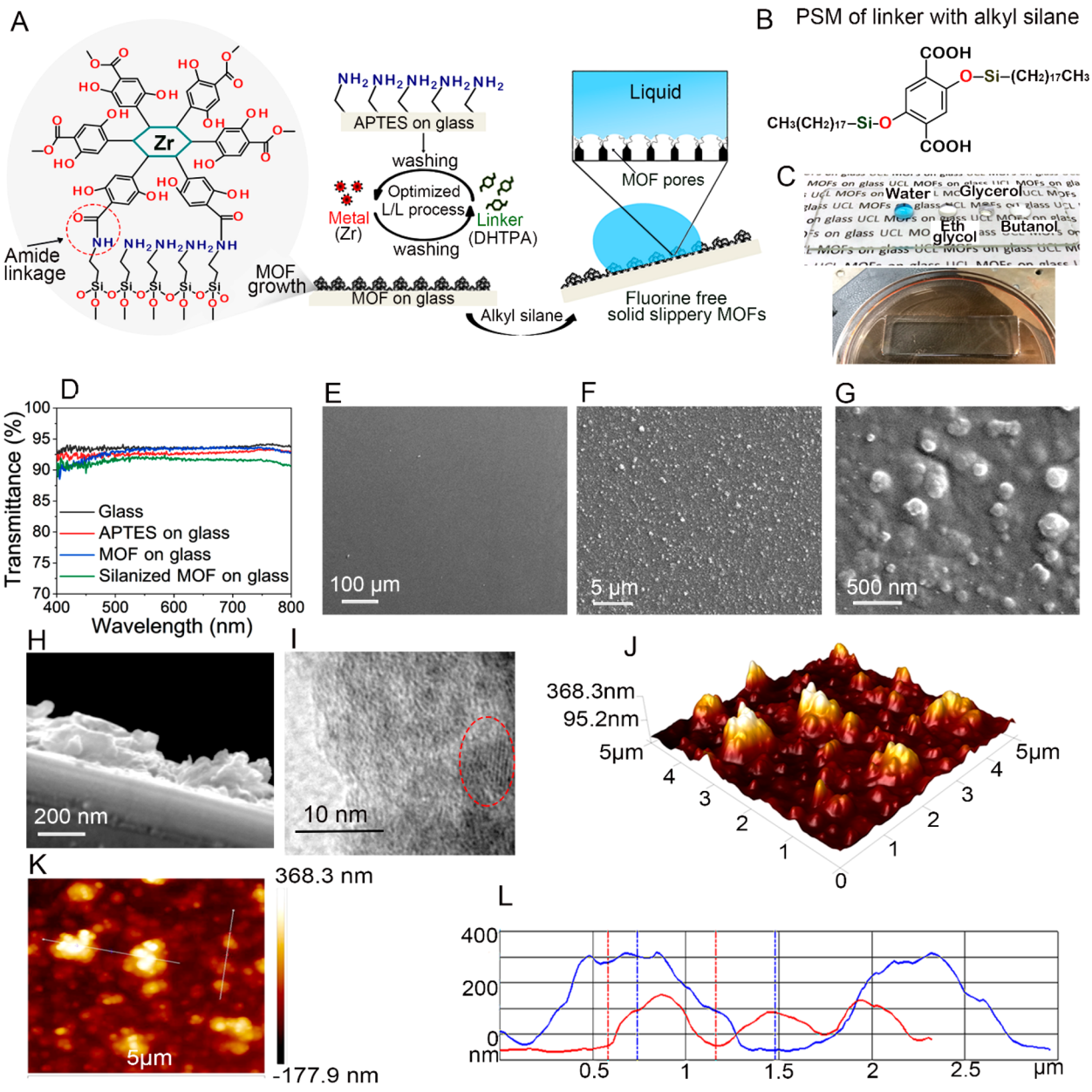

Figure 1. Fabrication, concept, and morphological characterization of the nanohierarchical (rough) slippery MOF-based amphiphobic surface. (A) Schematic showing the L/L approach to obtain nanohierarchical MOFs on 3-aminopropyl-triethoxysilane (APTES)-functionalized glass through covalent amide linkage. (B) Postsynthetic alkyl silane functionalization exploiting the hydroxyl group in the dihydroxyterepthalic acid linker lowered the surface energy. (C) Top: image showing droplets of water, glycerol, ethylene glycol, and butanol on the transparent nanohierarchical MOF-coated glass slide, Bottom: a coated slide floating on water. (D) Optical transparency of different samples. (E) SEM image of the MOF film at low magnification, (F, G) SEM images at higher magnifications showing MOF particles. (H) Cross-sectional SEM image of MOF layer on glass. (I) High-resolution TEM image of MOF cluster showing porous frameworks with approximately 1 nm pore size. The highly aligned crystal lattice structures are marked with a red ellipse. (J) 3D topography confirming nanoscale rough structures recorded by AFM. The larger nanoscale features combined with much smaller MOF pores (~1 nm scale) provide the nanohierarchical morphology. (K, L) The cross-sectional view of the nanostructure heights recorded along two white lines in (K).

of the powder form. Roy et al. coated the ethanolic dispersion of Zn-based hydrophobic MOFs onto glass substrate by immersion and showed the self-cleaning performance.[16] Sun et al. physically adsorbed the hydrophobic UIO-66 MOF onto a glass slide to record the contact angles.[17] These prior works on applications of hydrophobic MOF structures lack the basic requirement of mechanical stability and have relied on the MOF particles physically adsorbing on the substrates. On the other hand, the surface-grown thin films of MOFs have been explored only for semiconductor devices, optical sensors, and gas sensors applications.[18] Recently, such surface-grown hydrophilic MOFs were infused with water-repellent lubricants to obtain slippery liquid-infused porous surfaces (SLIPS) with low contact angle hysteresis and anti-icing characteristics.[19] However, such SLIPS-based surfaces are susceptible to depletion of the lubricant liquid, with considerable efforts being directed to overcome this issue.[20] Additionally, achieving high-speed liquid impact resistance and low mobility of sliding drops on such SLIPS surfaces is a major challenge.[21] The surfaces presented here overcome these key challenges. To the

https://doi.org/10.1021/acs.nanolett.1c00157
Nano Lett. XXXX, XXX, XXX−XXX

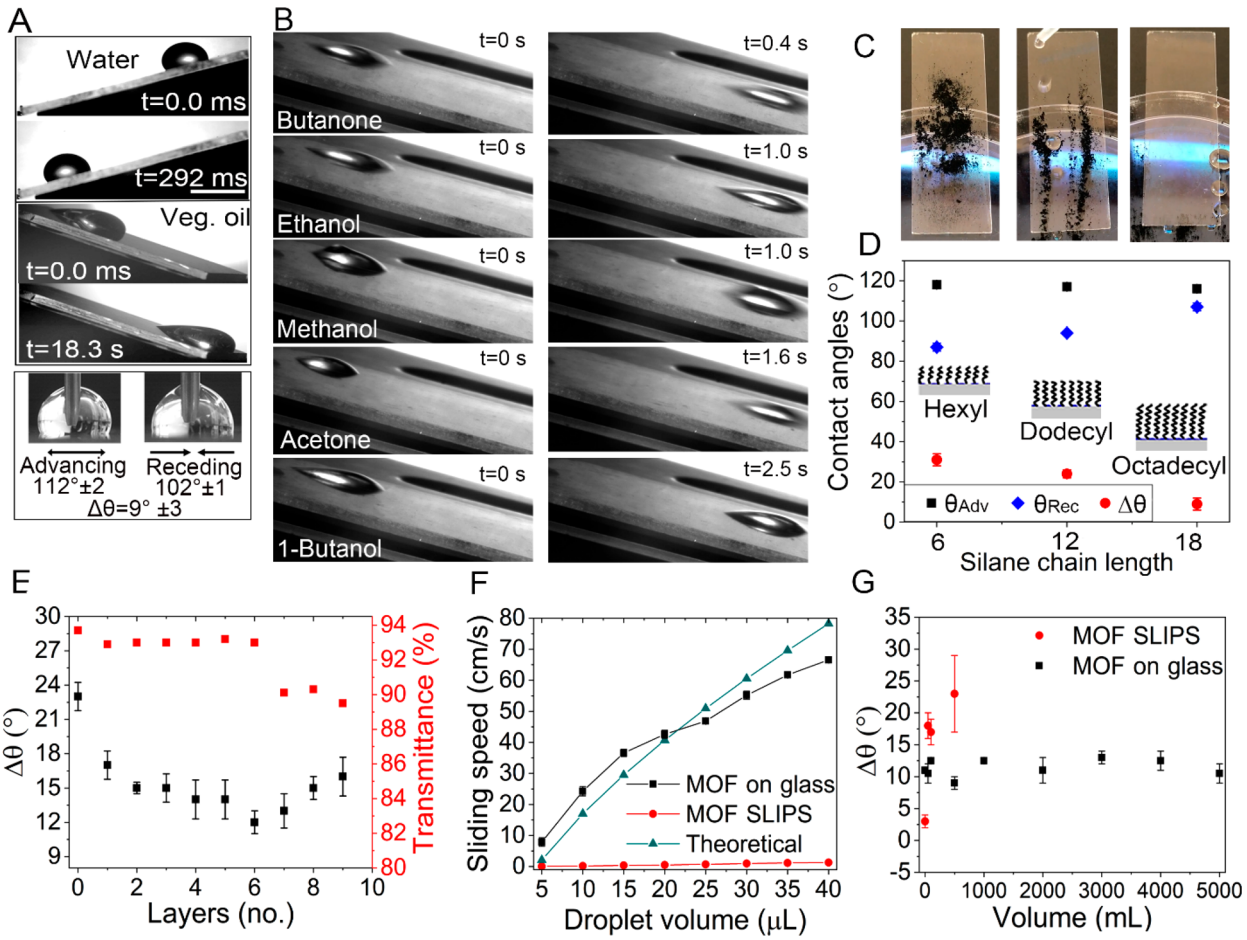

Figure 2. Optimization and assessment of liquid mobility on the nanohierarchical amphiphobic MOF surfaces. (A) Photographs capturing water and vegetable oil droplets sliding at 15° surface tilt and advancing and receding angles of a water droplet. (B) Image sequence showing the amphiphobicity of the nanohierarchical surface through sliding of low surface tension liquids at 15° tilt angles. The low surface tension liquids are arranged with increasing viscosity (from top to bottom), which affects the sliding speed. (C) Self-cleaning process of the surface showing dirt removal by sliding water droplets. (D) Effect of silane chain length on water advancing, receding, and hysteresis angles. Insets illustrate the silane chains and their IUPAC names. (E) Optimising number of MOF layers for a trade-off between transparency and wetting hysteresis. (F) Drop sliding speeds on the slippery nanohierarchical MOFs compared against with theoretical velocities and those measured on a comparative SLIPS. (G) Comparative change in hysteresis angles through continuous dripping of water droplets.

best of our knowledge, no work on the surface-grown transparent and hydrophobic MOF film has been reported thus far and, as we will show below, our work also offers some important advances in terms of all-round functionality of the resulting surfaces.

For our nanohierarchical MOF film, a precise, layer-by-layer (L/L) approach was adopted to achieve a careful trade-off between roughness, mechanochemical stability, and light transmittance (Figures S1−S6). The nanohierarchical morphology was comprised of tens to hundreds of nanometer-sized MOF particles and the individual MOF pores at a ∼1 nm scale. Postsynthetic modification with alkyl silanes rendered the surface amphiphobic (Figure 1B, *c.f.*, the effect of silane chain variation tested below). The optimal surface exhibited ≥92% transmittance throughout the visible spectrum (Figure 1C and 1D). The MOF crystallinity was confirmed by powder X-ray diffraction (Figure S1).[22] The chemical structure was confirmed[23] by FTIR (Figure S2) with specific peaks around 1435 and 1563 cm^{-1}, by Raman spectra (Figure S2) with peaks around 850, 1150, and 1600 cm^{-1}, and by the uniformity of elemental distribution using SEM-EDS (Figure S4). Figure 1E−G show the surface morphology imaged using a scanning electron microscope (SEM); the higher magnification images capture the MOF nanoparticle sizes (tens to hundreds of nanometers). We tracked MOF growth using SEM (Figure S5); after the first 2−3 layers, the films remained smooth and uniform. Beyond the third layer, the roughness started increasing. To maintain high transparency, 6 layers were optimal; beyond 8−9 layers, the transmittance started falling. The cross-section of the MOF on glass, shown in Figure 1H, confirms the nanoroughness and a film thickness of ∼200 nm, in agreement with ellipsometry which yielded a thickness and refractive index of 165 nm and ∼1.5, respectively. The mechanically scratched powder was imaged using a transmission electron microscope (TEM); the microporous structure of the MOF film was clear at high magnification (Figure 1I). Figure 1J−L shows the 3D topology of the 6-layer nanohierarchical MOF imaged using an atomic force microscope (AFM); the root mean square roughness was ∼73.9 nm, and the maximal height of the MOF clusters ranged from ∼100 nm to ∼300 nm.

The functionalized nanohierarchical MOF films offered a rough but slippery surface on which water, vegetable oil, alcohols, and ketones slid off easily at ≤20° angles (Videos S1

https://doi.org/10.1021/acs.nanolett.1c00157
Nano Lett. XXXX, XXX, XXX−XXX

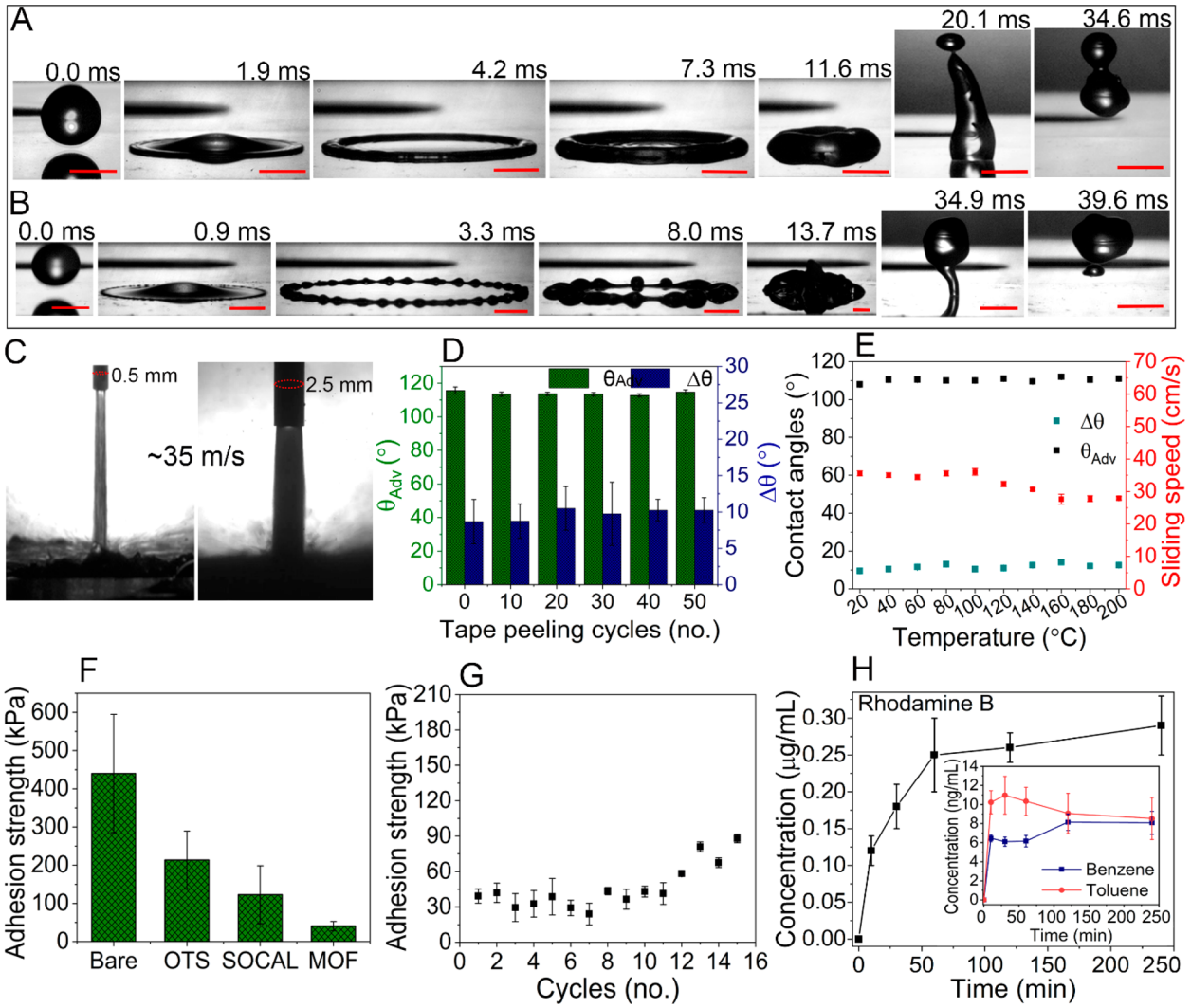

Figure 3. Surface robustness and usage potential. (A) Time-lapse snapshots (scale = 2 mm) of drop impact on the nanohierarchical slippery MOF surfaces at 1.4 m/s and (B) 4.2 m/s impact velocities. (C) Water jets (nozzle diameter = 0.5 and 2.5 mm) impacting at ~35 m/s. (D) The effect of tape peel cycles; θ_A, θ_R, and $\Delta\theta$ remained unchanged even after 50 repeated cycles. (E) Thermal stability test of the surface. (F) Ice adhesion strength of different treatments on glass substrate including bare glass as a control, glass functionalized with trichlorooctadodecyl silane (OTS), an ultrasmooth surface based on polydimethylsiloxane oligomers[4] (SOCAL), and our nanohierarchical MOF surfaces. (G) Change in the ice adhesion strength of the MOF surface with up to 15 repeated icing/deicing cycles. (H) Pollutant adsorption in the MOF surface, where the main graphs show rhodamine B adsorption; benzene and toluene cases are shown in the insert.

and S2). The reduced solid fraction (ϕ) of ~0.4 for the MOF surface (Supporting Information) compared to a smooth hydrophobic surface helped achieve the low hysteresis and sliding angles against water and other low surface tension liquids. The contribution of low ϕ could be clearly appreciated from the enhancement in advancing angle of the water droplet from ~102° on the glass substrate modified with the same silane to ~112° on the hydrophobic MOF film.

A free sliding of vegetable oil was observed at 15° (Figure 2A), and the surface also showed repellency to alcohols or polar liquids but not to nonpolar hydrocarbons (due to alkyl functionalization). Butanone (23.9 mN/m), ethanol (22.1 mN/m), methanol (22.5 mN/m), acetone (25.2 mN/m), 1-butanol (25 mN/m), 1-decanol (28.5 mN/m), glycol (47. mN/m), cyclohexanol (33.4 mN/m), and 1,2-butanediol (37.2 mN/m) were also tested and slid off at 15° inclination (Figure 2B and Figure S8). Carbon powder was easily removed by water drops sliding off the surface, confirming the self-cleaning property (see Figure 2C and Video S3).

To understand the sliding behavior, functionalization using trichlorohexylsilane (C_6, ~0.924 nm), trichlorododecyl silane (C_{12}, ~1.84 nm), and trichlorooctadecyl silane (C_{18}, ~2.77 nm) was investigated. The functionalized samples were evaluated by measuring advancing (θ_A) and receding (θ_R) contact angles of water droplets and the hysteresis ($\Delta\theta$), calculated using ($\Delta\theta = \theta_A - \theta_R$). Figure 2D shows that θ_A remained approximately constant and θ_R increased with the carbon chain length of the silanes, yielding a hysteresis of 9° ± 2° for the octadecyl silane. The possible reason for the significant decline in the hysteresis is a combination of the shallow nanohierarchical morphology and the known flexibility[24−26] of the grafting chains on the MOF surface. The nanohierarchical morphology with the ~1 nm pores and the associated high capillary pressure, resisting liquid meniscus penetration, reduce the solid−liquid contact and facilitate easy sliding of the droplets. Previously, such amphiphobic slippery behavior has been reported only either for lubricant-infused surfaces[27] or ultrasmooth substrates.[4] Given the shallowness of

https://doi.org/10.1021/acs.nanolett.1c00157
Nano Lett. XXXX, XXX, XXX−XXX

roughness, a droplet meniscus should sag into the gaps between the particle clusters on our nanohierarchical surface, whereas the penetration into the MOF pores will be difficult due low surface energy and the ∼1 nm size; clearly our surfaces are also unlike superoleophobic surfaces.[28] Wong and co-workers infused the lubricants into micro- and nanoscale textures and showed that an immiscible liquid droplet, similar to the working principle of the liquid-infused surfaces in general, can slide in Wenzel state as well.[29−31] Our nanohierarchical morphology and optimal length of the alkyl chain, with its associated flexibility, enable a slippery nano-Wenzel state without any liquid infusion (see the schematic in Figure 1A, right). The combination of the nanohierarchical morphology and alkyl chain is important for the excellent droplet mobility and liquid impact resistance, which is to be presented later.

For transparency, beyond 6 MOF layers the hysteresis started to increase (see Figure 2E and Figure S9). Silanized glass is shown as the 0-layer case in Figure 2E. To quantify the surface's slippery behavior, it was placed at a 30° tilt angle and the sliding speeds were measured for droplets with different volumes; the data are plotted in Figure 2F. As expected[32] (Supporting Information), a linear increase in the sliding speed from 7.8 ± 1 cm/s to 66.5 ± 1 cm/s was observed with a change in droplet volume from 5 and 40 μL (Figure 2F). For comparison, the nanohierarchical MOF was infused with a lubricant (silicone oil, 500 cSt) to obtain a slippery liquid-infused porous surface (i.e., a SLIPS equivalent of our surfaces). The droplet sliding speed on SLIPS, despite its relatively small hysteresis, was 10-fold lower, underscoring the excellent liquid mobility of our nanohierarchical surfaces (Figure 2F). The relative robustness of the nanohierarchical MOF surfaces compared to SLIPS was also tested by dripping water droplets continuously onto the surfaces at 1 L/h, using a syringe pump (Supporting Information). Our nanohierarchical MOF showed excellent stability with no change in hysteresis, whereas a rapid increase in hysteresis from ∼4° to ∼23° was observed on the SLIPS due to oil depletion (Figure 2G).

Drop impacts at 1.4 and 4.2 m/s (drop diameter = ∼2.7 mm), with relatively low and high contribution of impact kinetic energy, were used to investigate low-speed liquid impacts. Videos from a high-speed camera are presented in Video S4, and the stages in impact dynamics are shown in Figure 3A and Figure 3B. The droplets bounced off the MOF surface and roughly took the same time irrespective of the impact velocity. However, the impact velocities of 1.4 and 4.2 m/s led to spreading diameters of ∼1.0 and ∼1.5 cm, respectively, and hydrodynamic instability in the rim was observed for the latter. The silanized bare glass surface showed no bounce off (Figure S10). Next, high-speed jet impact tests were performed (see Figure 3C and Supporting Information) to assess the surface liquid impalement resistance. The transparent MOF surface resisted impalement at the maximum jet speed attainable in our setup (>35 m/s, corresponding maximum liquid Weber number ∼42500), even after repeated tests. The videos from a high-speed camera and an ordinary camera are presented in Videos S5 and S6 and in Video S7, respectively. After repeated jet impacts, no surface damage was observed (Figure S11). This was also confirmed by placing a water droplet at the location of impact and ensuring normal sliding (Figure S13 and Video S8).

Next, mechanical robustness was tested using tape peel (Figure S15) and pencil hardness (Figure S16) tests. A high-tack tape (3M VHB 5952 with a strong adhesive peel strength of 3900 N/m) was pressed on the surface with a 2 kg roller, before it was then peeled off to complete one peel cycle (Figure S15). No significant change in the contact angles and hysteresis was observed even after 50 repetitive cycles (Figure 3D). Following the tape peel, the surface was also tested using drop impact (1.2 m/s) (Figure S16 and Video S9) and morphological characterization (Figure S18) to confirm robustness. The scratch resistance was checked through standard pencil hardness test (Figure S16). The coating demonstrated excellent stability against HB to 5H pencil scratch. The stability was assessed by monitoring contact angle hysteresis and droplets sliding (Video S10).

Chemical stability was tested next by immersing the coatings in strongly acidic and basic media (Figure S19A and S19B), and the stability ranged from several hours (in base) to a month (in acid). The slippery MOF surface also demonstrated good thermal stability up to 200 °C (Figure 3E). The sample was heated for 60 min at each temperature followed by cooling to room temperature and measurement of the wetting angles and the sliding speed. The surface maintained the hydrophobicity and suffered an only slight decline in the sliding speed from ∼35 to ∼30 cm/s.

We also evaluated our surface for its ice adhesion (Supporting Information). Bare glass and glass functionalized with the same silane used to functionalize the MOF were used as references. Additionally, ultrasmooth polydimethylsiloxane oligomers (SOCAL)-treated glass[4] was also used. The lowest ice adhesion strength of 35 ± 10 kPa was recorded on the nanohierarchical MOF surface (Figure 3F). Whereas, the ice adhesion strength on hydrophilic MOFs (prior to functionalization) was measured to be 100.5 ± 5 kPa. The surface robustness was tested by repeating icing/deicing cycles; no change in the ice adhesion strength was observed up to 11 cycles (Figure 3G). The morphology changed noticeably after 15 icing/deicing cycles and showed some cracks in coating (Figure S21). The inherent adsorption efficacy[33] of MOFs was exploited to demonstrate the potential of nanohierarchical MOF surfaces for cleaning some of the most common and hazardous pollutants[34] such as rhodamine B, benzene, and toluene. Our surface showed excellent and quick adsorption of rhodamine B (∼0.77 μg/cm^2), benzene (∼21.7 ng/cm^2), and toluene (∼29.2 ng/cm^2) (Figure 3H and Figure S22). Overall, the multifunctionality presented shows the potential usage of the presented nanohierarchical MOF coating in applications such as windows, hand-held displays, goggles, wind screens, and so on.

■ ASSOCIATED CONTENT

Supporting Information

The Supporting Information is available free of charge at https://pubs.acs.org/doi/10.1021/acs.nanolett.1c00157.

Descriptions of materials, surface fabrication methods, and functionalization; wettability testing details; solid fraction calculation; mechanical, chemical, and thermal stability details; jet impact and icing chamber setup details; pollutant adsorption method; and captions for Videos S1−S10 (PDF)

Video S1 (MP4)

Video S2 (MP4)

Video S3 (MP4)

Video S4 (MP4)

https://doi.org/10.1021/acs.nanolett.1c00157
Nano Lett. XXXX, XXX, XXX−XXX

Video S5 (MP4)
Video S6 (MP4)
Video S7 (MP4)
Video S8 (MP4)
Video S9 (MP4)
Video S10 (MP4)

AUTHOR INFORMATION

Corresponding Author

Manish K. Tiwari − *Nanoengineered Systems Laboratory, UCL Mechanical Engineering, University College London, London WC1E 7JE, U.K.; Wellcome/EPSRC Centre for Interventional and Surgical Sciences, University College London, London W1W 7TS, U.K.;* orcid.org/0000-0001-5143-6881; Email: m.tiwari@ucl.ac.uk

Authors

Vikramjeet Singh − *Nanoengineered Systems Laboratory, UCL Mechanical Engineering, University College London, London WC1E 7JE, U.K.*

Xuehu Men − *Nanoengineered Systems Laboratory, UCL Mechanical Engineering, University College London, London WC1E 7JE, U.K.*

Complete contact information is available at: https://pubs.acs.org/10.1021/acs.nanolett.1c00157

Notes

The authors declare no competing financial interest.

ACKNOWLEDGMENTS

We thank Mark Portnoi and Ioannis Papakonstantinou for help with transparency and ellipsometry measurements and Dr. Kersti Karu for mass spectrometry. Funding from the European Union's Horizon 2020 Research and Innovation programme under grant 801229 (HARMoNIC) and the European Research Council (ERC) grant 714712 (NICE-DROPS) is gratefully acknowledged.

REFERENCES

(1) Deng, X.; Mammen, L.; Butt, H. J.; Vollmer, D. Candle soot as a template for a transparent robust superamphiphobic coating. *Science* **2012**, *335* (6064), 67−70.

(2) Yong, J.; Chen, F.; Yang, Q.; Huo, J.; Hou, X. Superoleophobic surfaces. *Chem. Soc. Rev.* **2017**, *46* (14), 4168−4217.

(3) Maitra, T.; Tiwari, M. K.; Antonini, C.; Schoch, P.; Jung, S.; Eberle, P.; Poulikakos, D. On the nanoengineering of superhydrophobic and impalement resistant surface textures below the freezing temperature. *Nano Lett.* **2014**, *14* (1), 172−182.

(4) Wang, L.; McCarthy, T. J. Covalently attached liquids: instant omniphobic surfaces with unprecedented repellency. *Angew. Chem., Int. Ed.* **2016**, *55* (1), 244−248.

(5) Chen, W.; Zhang, P.; Zang, R.; Fan, J.; Wang, S.; Wang, B.; Meng, J. Underwater superoleophobicity: nacre-inspired mineralized films with high transparency and mechanically robust underwater superoleophobicity. *Adv. Mater.* **2020**, *32*, 1907413.

(6) Li, X.; Wang, D.; Tan, Y.; Yang, J.; Deng, X. Designing transparent micro/nano re-entrant-coordinated superamphiphobic surfaces with ultralow solid/liquid adhesion. *ACS Appl. Mater. Interfaces* **2019**, *11* (32), 29458−29465.

(7) Teisala, H.; Geyer, F.; Haapanen, J.; Juuti, P.; Makela, J. M.; Vollmer, D.; Butt, H. J. Ultrafast processing of hierarchical nanotexture for a transparent superamphiphobic coating with extremely low roll-off angle and high impalement pressure. *Adv. Mater.* **2018**, *30*, 1706529.

(8) Wang, D.; Sun, Q.; Hokkanen, M. J.; Zhang, C.; Lin, F. Y.; Liu, Q.; Zhu, S. P.; Zhou, T.; Chang, Q.; He, B.; Zhou, Q.; Chen, L.; Wang, Z.; Ras, R. H. A.; Deng, X. Design of robust superhydrophobic surfaces. *Nature* **2020**, *582* (7810), 55−59.

(9) Kalmutzki, M. J.; Hanikel, N.; Yaghi, O. M. Secondary building units as the turning point in the development of the reticular chemistry of MOFs. *Sci. Adv.* **2018**, *4*, No. eaat9180.

(10) Wu, H. B.; Lou, X. W. Metal-organic framework and their derived materials for electrochemical energy storage and conversion: promises and challenges. *Sci. Adv.* **2017**, *3*, No. eaap9252.

(11) Dang, S.; Zhu, Q. L.; Xu, Q. Nanomaterials derived from metal-organic frameworks. *Nat. Rev. Mater.* **2018**, *3*, 17075.

(12) Wu, H.; Yildirim, T.; Zhou, W. Exceptional mechanical stability of highly porous zirconium metal−organic framework UiO-66 and its important implications. *J. Phys. Chem. Lett.* **2013**, *4* (6), 925−930.

(13) Redfern, L. R.; Farha, O. K. Mechanical properties of metal−organic frameworks. *Chem. Sci.* **2019**, *10* (46), 10666−10679.

(14) Jayaramulu, K.; Geyer, F.; Schneemann, A.; Kment, S.; Otyepka, M.; Zboril, R.; Vollmer, D.; Fischer, R. A. Hydrophobic metal−organic frameworks. *Adv. Mater.* **2019**, *31*, 1900820.

(15) Mukherjee, S.; Sharma, S.; Ghosh, S. K. Hydrophobic metal-organic frameworks: Potential toward emerging applications. *APL Mater.* **2019**, *7*, 050701.

(16) Roy, S.; Suresh, V. M.; Maji, T. K. Self-cleaning MOF: realization of extreme water repellence in coordination driven self-assembled nanostructures. *Chem. Sci.* **2016**, *7*, 2251.

(17) Sun, D.; Adiyala, P. R.; Yim, S.-J.; Kim, D.-P. Pore-surface engineering by decorating metal-oxo nodes with phenylsilane to give versatile super-hydrophobic metal−organic frameworks (MOFs). *Angew. Chem., Int. Ed.* **2019**, *58*, 7405−7409.

(18) Xiao, Y.-H.; Gu, Z.-G.; Zhang, J. Surface-coordinated metal−organic framework thin films (SURMOFs) for electrocatalytic applications. *Nanoscale* **2020**, *12*, 12712−12730.

(19) Gao, J.; Zhang, Y.; Wei, W.; Yin, Y.; Liu, M.; Guo, H.; Zheng, C.; Deng, P. Liquid-infused micro-nanostructured MOF coatings (LIMNSMCs) with high anti-icing performance. *ACS Appl. Mater. Interfaces* **2019**, *11*, 47545−47552.

(20) Peppou-Chapman, S.; Hong, J. K.; Waterhouse, A.; Neto, C. Life and death of liquid-infused surfaces: a review on the choice, analysis and fate of the infused liquid layer. *Chem. Soc. Rev.* **2020**, *49*, 3688−3715.

(21) Peng, C.; Chen, Z.; Tiwari, M. K. All-organic superhydrophobic coatings with mechanochemical robustness and liquid impalement resistance. *Nat. Mater.* **2018**, *17*, 355−360.

(22) Kandiah, M.; Nilsen, M. H.; Usseglio, S.; Jakobsen, S.; Olsbye, U.; Tilset, M.; Larabi, C.; Quadrelli, E. A.; Bonino, F.; Lillerud, K. P. Synthesis and stability of tagged UiO-66 Zr-MOFs. *Chem. Mater.* **2010**, *22*, 6632−6640.

(23) Liu, J.; Wöll, C. Surface-supported metal−organic framework thin films: fabrication methods, applications, and challenges. *Chem. Soc. Rev.* **2017**, *46*, 5730−5770.

(24) Sohn, E. H.; Ahn, J.; Kim, B. G.; Lee, J. C. Effect of n-alkyl and sulfonyl groups on the wetting properties of comblike poly(oxyethylene)s and stick−slip behavior. *Langmuir* **2011**, *27* (5), 1811−1820.

(25) Perera, H. J.; Mortazavian, H.; Blum, F. D. Surface properties of silane-treated diatomaceous earth coatings: effect of alkyl chain length. *Langmuir* **2017**, *33* (11), 2799−2809.

(26) García, N.; Benito, E.; Guzman, J.; Tiemblo, P. Use of p-toluenesulfonic acid for the controlled grafting of alkoxysilanes onto silanol containing surfaces: preparation of tunable hydrophilic, hydrophobic, and super-hydrophobic Silica. *J. Am. Chem. Soc.* **2007**, *129* (16), 5052−5060.

(27) Wong, T. S.; Kang, S. H.; Tang, S. K. Y.; Smythe, E. J.; Hatton, B. D.; Grinthal, A.; Aizenberg, J. Bioinspired self-repairing slippery surfaces with pressure-stable omniphobicity. *Nature* **2011**, *477* (7365), 443−447.

(28) Herminghaus, S. Roughness-induced non-wetting. *Europhys. Lett.* **2000**, *52*, 165−170.

(29) Dai, X.; Stogin, B. B.; Yang, S.; Wong, T. S. Slippery Wenzel state. *ACS Nano* **2015**, *9* (9), 9260−9267.
(30) Dai, X.; Sun, N.; Nielsen, S. O.; Stogin, B. B.; Wang, J.; Yang, S.; Wong, T. S. Hydrophilic directional slippery rough surfaces for water harvesting. *Sci. Adv.* **2018**, *4*, No. eaaq0919.
(31) Huang, Y.; Stogin, B. B.; Sun, N.; Wang, J.; Yang, S.; Wong, T. S. A switchable cross-species liquid repellent surface. *Adv. Mater.* **2017**, *29*, 1604641.
(32) Yilbas, B. S.; Al-Sharafi, A.; Ali, H.; Al-Aqeeli, N. Dynamics of a water droplet on a hydrophobic inclined surface: influence of droplet size and surface inclination angle on droplet rolling. *RSC Adv.* **2017**, *7* (77), 48806−48818.
(33) DeChellis, D. M.; Ngule, C. M.; Genna, D. T. Removal of hydrocarbon contaminants from water with perfluorocarboxylated UiO-6X derivatives. *J. Mater. Chem. A* **2020**, *8*, 5848−5852.
(34) Palomino Cabello, C.; Picó, M. F. F.; Maya, F.; del Rio, M.; Turnes Palomino, G. UiO-66 derived etched carbon/polymer membranes: High-performance supports for the extraction of organic pollutants from water. *Chem. Eng. J.* **2018**, *346*, 85−93.

https://doi.org/10.1021/acs.nanolett.1c00157
Nano Lett. XXXX, XXX, XXX−XXX